Variations of extreme precipitation events with sub-daily data: a case study in the Ganjiang river basin

Guangxu Liu[1*], Aicun Xiang[1], Zhiwei Wan[1], Yang Zhou[2], Jie Wu[1], Yuandong Wang[1], Sichen Lin[1]

[1]School of Geography and Environmental Engineering, Gannan Normal University, Ganzhou 341000, China
[2]Department of Agricultural Economics and Rural Development, Renmin University of China, Beijing 100872, China

Correspondence to:Guangxu Liu (lg760411@126.com)

Abstract Climate warming increases the intensity of extreme precipitation. Studying extreme precipitation patterns and changes is vital to reducing risk. This paper investigates thresholds, changes and time scales for extreme precipitation using sub-daily records from meteorological stations in the Ganjiang River basin. We use the gamma distribution and select the L-moment method to estimate the parameters α and β. Results show that (1) continuous precipitation events of 36 hours contributed the most precipitation to the total but with lower frequency, which would be key events for flood monitoring; (2) The intensity and the occasional probability of extreme precipitation will increase in spring in the future in stations like Yifeng, Zhangshu and Ningdu, which will in turn increase the risk of storm floods; (3) spatial distribution of extreme precipitation risk shows that the risk increases as elevation increases in the northern lowland and the Jitai Basin in the mid-stream region, while the risk in the southern mountainous region decreases with elevation increasing. These findings will facilitate emergency preparedness, including risk management and disaster assistance in the study areas.

Key words: Extreme precipitation, gamma distribution, L-moment method, the Ganjiang River

1 Introduction

The hydrological cycle is expected to intensify with global warming, which likely increases the intensity of extreme precipitation events and the risk of flooding (Tabari, 2020). Extreme weather events such as storms have occurred frequently around the world in recent years, which often cause disastrous floods and landslides, resulting in great casualties and economic losses. Zhengzhou city in China experienced a rare and continuous heavy precipitation process from July 18th to July 21st in 2021. Extreme precipitation intensity reached 201.9 mm in an hour and cumulative precipitation reached 449 mm, which caused 292 deaths and 47 missing, 65.5 billion yuan lost and 44,209.73 hectares of crops affected. Eight days before the Zhengzhou storm, parts of Rhineland-Palatinate and North Rhine-Westphalia in Germany were also encountered heavy precipitation of 148 litres of rain per square meter within 48 hours, causing severe flash flooding. As of July 23, 2021, the death toll from the flood in western Germany reached 180 people and about 150 people were missing. The reconstruction funds reached billions of euros. Changes in extreme precipitation are among the most impact-relevant consequences of climate warming (Pfahl et al., 2017). IPCC reported that the globally averaged combined land and ocean surface

temperature showed a warming trend of 0.85 °C [0.65 °C to 1.06°C] over the period 1880 to 2012 and continued emission of greenhouse gases will cause further warming in the future (Pachauri et al., 2014). The continuous warming breaks the original energy balance of the climate system, causing abnormalities in the atmospheric circulation and water circulation system, which in turn causes an increase in extreme precipitation events and discharges. Theoretical models predict that extreme precipitation intensity could exponentially increase with warming at a rate determined by the Clausius–Clapeyron (C–C) relationship (Trenberth, 1999; Trenberth et al., 2003). An increase in the frequency of extreme precipitation events has increased at the high and mid-latitudes of the land as a likely consequence of climate warming (Rodrigo, 2010). A rate of 6% to 10% increase per degree of warming has been observed in annual maximum daily precipitation over land (Asadieh et al., 2015; Westra et al., 2013). Climate models show that extreme precipitation will continue to increase in the 21st century at approximately the same rate because of continued warming (Fischer et al., 2013; O'gorman et al., 2009; Pendergrass and Hartmann, 2014; Sillmann et al., 2013). The future trend of extreme precipitation in China is consistent with that of the world. Xiao et al. found that analysis from gauge records for 1971–2013 from 721 weather stations showed that the maximum hourly summer rainfall intensity has increased by about 11.2% on average in China which will exacerbate the risks of flash floods in rapidly urbanizing areas (Xiao et al., 2016). Zeng and Lu found that summer precipitation in China from 1961 to 2010 experienced the biggest increase in the middle and lower reaches of the Yangtze River (Zeng and Lu, 2015), which was caused mainly by the positive contribution of extreme precipitation (Shi et al., 2014). Gao and Xie analyzed the response of extreme precipitation to warming in winter in China and found that extreme precipitation would increase by 22.6% for every 1°C increase in winter temperature. This increase is significantly higher than the global average, indicating that extreme precipitation is more sensitive to warming in winter in China (Gao and Xie, 2014). Wu et al. analyzed the changes of extreme weather events under the background of future warming and pointed out that compared with 1986-2005, the total annual precipitation (PROPTOT), the five-day maximum precipitation (Rx5day), the heavy precipitation (R95p) would increase in China (Wu et al., 2015). The CMIP5 data also show a trend of increasing extreme precipitation events in the future in various regions of China (Zhao et al., 2019). These studies show the importance of studying extreme precipitation changes and trends under climate warming.

Extreme precipitation can be defined in a variety of ways. Pendergrass thinks that extreme events can be considered if precipitation falls more than those which are often appreciated (Pendergrass, 2018). The expert Team on Climate Change Detection Monitoring Indices (ETCCDMI) established several indicators such as CWD10, CWD20, R1 day (annual), R10 mm and R20 mm in undertaking regional analysis for understanding climate extremes and trends (Easterling et al., 2003). Soro et al. grouped extreme events into two broad categories. One is the yearly extreme events, based on heavy daily rainfall. The other is event-driven extremes characterized by severe floods (Soro et al., 2016). A common definition of extreme precipitation is defined by an event passes a threshold of exceedance or a certain threshold. There are different criteria to define the threshold, including a fixed absolute value (Brunetti, Maugeri et al. 2004; López-Moreno and Beniston 2009), standard deviation based on statistics and percentile-based thresholds (Fernández-Montes, Seubert et al. 2014; Merino,

Fernández-Vaquero et al. 2016). Practically, percentile-based thresholds such as 95th or 99th percentile of the cumulative frequency distribution of daily precipitation with only wet days (or wet hours) is widely used in previous studies (Marelle, Myhre et al. 2018; Merino, Fernández-González et al. 2018; Pendergrass 2018; Myhre, Alterskjær et al. 2019). Pendergrass points out that how we define extreme precipitation affects the conclusions we draw. The reason why researchers focus on extreme precipitation is because extreme precipitation is one of the most frequent weather factors resulting in floods and landslides which are hazards responsible for damage to buildings and infrastructures, serious social disruption, and loss of human life worldwide each year (Soro et al., 2016). The choice of extreme definition depends on the intended use in terms of reducing disaster loss.

In specific research, researchers used either precipitation observations or simulated data from climate models to study the temporal and spatial variation of the scale and frequency of extreme precipitation. For example, Gao et al. examined the space-time variations of extreme precipitation over monsoon regions in China and assessed the time-varying influences of climate drivers using Bayesian dynamic linear regression. Results suggest that the central-east and south China is dominated by less frequent but more intense precipitation (Gao et al., 2017). Ren et al. used the 0.5°×0.5° daily precipitation data from 1961 to 2011 in the National Meteorological Information center and the daily precipitation observations from the meteorological stations in China to investigate changes of extreme precipitation events in South China. The selected index includes the maximum five-day precipitation (RX5day), extreme precipitation (R95), days with precipitation ≥ 20mm (R20mm), continuous precipitation days (CWD) and intensity of daily precipitation (SDII), which are all recommended by the World Meteorological Organization. They found that RX5day, R95, R20mm and SDII have an inter-annual tendency rate of 0.17 mm a^{-1}, 1.14 mm·a^{-1}, 0.02 d^{-1}·a^{-1} and 0.01 mm·d^{-1}·a^{-1} (d^{-1}·or a^{-1} is the abbreviation of per day or per year), respectively. The proportions of grid points with an increasing trend of RX5day, SDII, and R95 reach 60.85%, 75.32%, and 75.74% respectively (Ren et al., 2014). Pfahl et al. decompose the forced response of daily regional scale extreme precipitation in climate-model simulations into thermodynamic and dynamic contributions using a robust physical diagnostic to study the regional pattern of projected changes in extreme precipitation. Pfahl et al. found that thermodynamics alone would lead to a spatially homogeneous fractional increase in most regions throughout the globe. The dynamic contribution amplifies the increase in the Asian monsoon region but weakens them across the Mediterranean, South Africa and Australia. They think that the dynamic contribution is a key to reducing uncertainties in future projections of regional extreme precipitation (Pfahl et al., 2017). Mukherjee et al. studied the gridded observations and simulations from the coupled model inter-comparison project 5 (CMIP5) and climate of the 20th century plus (C20C+) detection and attribution (D & A) project. They found that the frequency and intensity of extreme precipitation events have increased in India during the last few decades and anthropogenic warming has made a significant contribution to the rise in the frequency (Mukherjee et al., 2018). Talchabhadel et al. analyzed the spatial distribution of monthly and annual precipitation, 1-day extreme precipitation and their trends with the records from 291 stations across Nepal for the period of 1966–2015. The result shows that extreme precipitation events has increased in western mountainous regions in the recent decades (Talchabhadel et al., 2018). Bao et

al. analyzed daily extreme precipitation events in several Australian cities and found that future daily extremes are increasing at rates faster than those inferred from observed scaling (Bao et al., 2017).

These studies use daily precipitation to analyze extreme events. However, events with scales shorter or longer than one day also cause floods. Merino et al. explained that daily databases would bring uncertainty in analysing floods with two examples (Merino et al., 2018). One example is that two extreme precipitation events with the same amount of precipitation but one event resulted in a flash flood due to its two hours' duration while the other one had no hydrologic floods because it lasted for over 12 consecutive hours. Another example is that a precipitation event below the extreme precipitation threshold posed floods because it began on one day and ended the next and the total amount was high but not recorded. It is key to analyze precipitation event periods, that is, the time scales of precipitation. Besides, extreme precipitation poses a threat to human society because they may cause floods leading to loss of life and property (Tabari and Willems, 2018). Regional differences often indicate whether extreme precipitation can cause flooding. For example, daily precipitation of 50mm may have a low impact on human society in flat or humid areas. However, it can lead to flash floods and even landslides and debris flows in mountainous or arid areas (Tabari and Willems, 2018). Time distribution patterns and return levels of extreme precipitation should be analyzed in risk research locally (Wu et al., 2018). Furthermore, engineering construction in disaster mitigation and prevention usually follows a standard design flood of a certain return period. With climate warming, the intensity of extreme precipitation has increased significantly. Projects constructed in accordance with past flood control standards have the risk of increased losses. According to the annual report of road flooding statistics, the annual direct economic loss of road infrastructure caused by flood damage has reached 10 to 30 billion yuan in China in the past 10 years (Li et al., 2014). Analysing the changing trend of extreme precipitation and proposing a design standard for future flooding preparedness is of great significance to improving the disaster prevention and mitigation system (Xu et al., 2014; Chen, 2015).

Collectively, this analysis focusses on the objectives as below: (1) to investigate the thresholds of extreme precipitation using sub-daily records in meteorological stations in the Ganjiang river basin; (2) to identify the changes and time scales of extreme precipitation using probability distribution and M-K test; (3) to explore the risk caused by extreme precipitation with different time scales and return periods in a case study.

2 Data and methods

2.1 Study area

The study area comprises the Ganjiang basin which is located with a longitude spanning from 113.74E-116.63E and latitude spanning from 24.57N-29.07N in the southeast of China (Figure 1). The drainage area is about 81,244 km². The Ganjiang River is the main stream which originates from the south and flows into the Poyang Lake in the north. Extreme precipitation in this watershed depends heavily on the windward mountains, the amount of precipitation and the timing of precipitation

timing. The topography is characterized with mountains mainly distributed in the south and alluvial plains in the north. The Jiulian mountain is the south-western boundary. The Wuyi Mountain forms the east border. The elevation is uplifting gradually from the north to the south-eastern end, which results in a higher precipitation in the mountainous north-western area and a lower rainfall zone in the central basin and lower reach in the north (Hu et al., 2013). In addition to moderating effects due to topographical changes, near-stationary fronts, monsoon and typhoon systems also control precipitation patterns. The average annual precipitation ranges between 1400 and 1600 mm (Li et al., 2017). Due to the long existence (hours to days) of near-stationary fronts over the basin, over 70% of the annual precipitation occurs during the period from April to June. Monsoon and typhoon rainstorms frequently occur between July and September. This area is characterized by a highly variable hydro-climate and flood-prone area in China. Fluvial floodplain deposition investigations indicate that the Ganjiang basin has experienced 18 floods during the past 130 years (Liu et al., 2018).

2.2 Precipitation Data

The precipitation data are collected from 12 national basic meteorological stations in Figure 1 supplied by the National Meteorological information center in China. These stations scatter from latitude 24.87N to 28. 60N and longitude 113.95E to 116.02E (Table 1). The highest station is Jinggangshan (Jgs) with an elevation of 843 meters above the sea level (m a.s.l) and the lowest one is Zhangshu (Zs) with an elevation of 30 m a.s.l. Four stations, Yifeng (Yf), Zs, Lianhua (Lh) and Longnan (Ln) began observing in 1951. Ningdu (Nd)) and the others all began at the end of 1950s. All these stations have been well maintained and managed since the 1950s. The original data include precipitation records from 8:00 to 20:00 during the days, precipitation from 20:00 to 08:00 the following day during the nights, and daily precipitation from 20:00 to 20:00 the following day. The data precision is 0.1 mm. Twelve-hours (12-H) precipitation was defined as precipitation records from 8:00 to 20:00 during days or precipitation from 20:00 to 08:00 the following day during nights and the data were selected from the original data between 1959-1-1 and 2016-12-31 with the purpose of keeping the data consistency. The suppliers assessed the data quality with several assay controls and detection limits. The erroneous or likely-erroneous data were all manually verified and corrected. Particular attention has been paid to problems such as changing points arising from inhomogeneities of data series, which were validated and corrected according to the methods supposed by Wang in 2008 (Wang, 2008) station by station. The change points were detected by integrating a Box-Cox power transformation procedure into a common trend two-phase regression model-based test (the transPMFred algorithm). The detected change points were adjusted with a quantile matching (QM) algorithm (Wang et al., 2010).

Then a precipitation event is determined by rainfall above the threshold of 0.1mm in 12 hours (12-H) from 8:00 to 20:00 in the day or 20:00 to 8:00 in the night in this paper. Considering the high seasonal variations of precipitation in the study area, the investigation was performed season by season. Therefore, the data was divided into four seasons, where winter data refers to the records in December, January, and February; spring, March, April, and May; summer, June, July, and August; and autumn, September, October, and November. Seasonal and annual average precipitation was calculated for each station

and listed in Table 2, which shows that the highest precipitation in most stations is found in spring, followed by summer,
autumn and winter. The stations located in the windward mountains have more annual precipitation, while the stations located in the plain areas have less precipitation. Jgx in the west has the highest annual precipitation.

2.3 Definition of extreme precipitation

The definition of extreme precipitation should be chosen with care and articulate it clearly (Pendergrass, 2018). Previous studies have discussed the definition of what constitutes an extreme event (Saidi et al., 2015). These definitions are grouped into two categories (Easterling et al., 2000).

(1) Extreme events are defined according to intensity such as yearly or seasonal maximum, CWD10, CWD20, R1 day (annual), R10 mm and R20 mm indices from the Expert Team on Climate Change Detection Monitoring Indices (ETCCDMI) (Soro et al., 2016). Yearly or seasonal maxima are one of the commonly used extreme value sampling. It generates annual maximum series whose sample size is identical with the number of years. Yet this definition does not include all extreme values because any second highest would be dropped out (Saidi et al., 2015).

(2) Events over a threshold (EOT), referred to as the extreme frequency (Haylock and Nicholls, 2000), is the other definition. EOT is characterized by physical expected hazards, such as floods or hurricanes. Pendergrass investigated thresholds such as the 99th percentile of the cumulative frequency distribution, the 95th percentile and the 90th percentile and found that the way to define extreme precipitation would affect the conclusions (Pendergrass, 2018).

The impact of extreme precipitation on human beings is to cause flood disasters which often occur several times in some years and are missing in other years. Therefore, a threshold of the 99th percentile is selected to define extreme precipitation in this paper, which is calculated based on all rainy events from 1959 to 2016. According to this threshold, 0-4 extreme precipitation events can be found in a year, which is very close to the number of flood disasters that the study area experienced

2.4 Method to analyze extreme precipitation events

The goal of the return period analysis is to estimate the value of the event magnitude corresponding to a given probability. How to accurately estimate the return period of extreme precipitation needs deterministic information with sufficient skill (El Adlouni and Ouarda, 2010). It could be precisely determined by frequency distribution if there were sufficiently long records of precipitation. In this study, there are 58 years of rainfall records, which forces us to use limited samples to estimate events with a chance of 1 in 100 years or even more, i.e., exceedance probabilities of one percent or more. The addressed problem is solved in practice by estimating probability distributions, which can estimate parameters of a distribution based on samples. Such distributions involving precipitation research mainly includes: Gamma, Generalized Extreme Value and Pearson type 3 distributions. Gamma distribution is one of the most popular models for describing precipitation (Papalexiou et al., 2013), which could provide the best fit for rainfall distribution (Şen and Eljadid, 1999).

Gamma distribution belongs to the exponential family (Papalexiou et al., 2013). It is used to fit positive data and it is a good representation of rainfall distribution. Assuming that the precipitation in a certain period is x, the probability density function that satisfies the Gamma distribution is

$$G(x) = \frac{1}{\beta^{\alpha}\Gamma(\alpha)}x^{\alpha-1}e^{-x/\beta} \tag{1}$$

Where α is the shape parameter, β is the scale parameter, and x is the precipitation records. *(α, β) > 0* when *x > 0* and *(x; α, β)* =0 when $x \leq 0$. $\Gamma(\alpha)$ is the Gamma function.

The L-moment method (LM), along with the moment and maximum likelihood methods, was often applied to samples taken from simulated gamma distribution (Kliche et al., 2008)**.** LM are linear combinations of order statistics (L-statistics) analogous to conventional moments and can be used to summarize the shape of a probability distribution (Hosking, 1990). LM of a probability distribution of random variable X is defined in terms of a linear combination of probability weighted moments (PWM) by Hosking (Hosking, 1990). LM have some advantages: they are less sensitive to outliers in the data, approximate their asymptotic normal distribution more closely, are nearly unbiased for all combinations of sample sizes and populations, and can characterize a wider range of probability distributions than conventional moments. As the literature of Vivekanandan (Vivekanandan, 2015), LM is used to sample the precipitation for determining parameters α and β in this paper. Sample L-moments can be computed as population L-moments of the sample. Assume that variable *X* follows a certain distribution function, and *n is* sample value of the observed variable *x*. The *n*-values are sorted in ascending order and $X_{j:n}$ is used to represent the *j*-th value, i.e. $X_{1:n} \leq$.precipitation$\leq X_{j:n} \leq$.precipitation $\leq X_{n:n}$. The sample L-moments of the first 2 orders in a finite sample of *n* observations are calculated as follows (Wang, 1996):

$$l_1 = b_0$$
$$l_2 = 2b_1 - b_0$$
$$b_0 = n^{-1}\sum_{j=1}^{n} x_{j:n} \tag{2}$$
$$b_1 = n^{-1}\sum_{j=2}^{n}\frac{j-1}{n-1}x_{j:n}$$

The L-mean, L-variation of the sample series are defined as follows:

$$l_1 = b_0$$
$$t_2 = l_2/l_1 \tag{3}$$

Then the shape parameter α is estimated with l_1 and l_2 with the equation below by iteration using recursion (Kliche et al., 2008):

$$\frac{1}{\sqrt{\pi}} \frac{\Gamma(\alpha_L + 3/2)}{\Gamma(\alpha_L + 2)} = \frac{l_2}{l_1} \tag{4}$$

where α_L is the LM estimate of α.

215   Once the shape parameter is determined, the estimator for the scale parameter is calculated from:

$$\beta_L = \frac{a_L + 1}{l_1} \tag{5}$$

Python programs are used to estimate the gamma distribution function of the precipitation events with these equations, as well as to estimate extreme precipitation thresholds.

2.5 Method for spatio-temporal changes

220   The Mann-Kendall non-parametric test (M-K test) is a statistical test widely used to detect monotonic trends in climatological data series. Two advantages of the M-K test were summed up by Soro et al (Soro et al., 2016) :

- Distribution-free. It does not need to assume any distribution function of the values.
- Low sensitivity to abrupt breaks in homogeneous time series. It does not need to censor missing data.

Precipitation is intermittent and highly scale-dependent (Sun and Stein, 2015). Therefore, The M-K test is used to analyze

225   the trends of extreme precipitation in seasons.

If X_i and X_j are the time series precipitation observations in chronological order, then the M-K Statistics S, $V(S)$ and standardized test statistics Z are calculated with the equation as follows (Ahmad et al., 2015):

$$S = \sum_{i=1}^{n-1} \sum_{j=i+1}^{n} sig(X_j - X_i)$$

$$sgn(X_j - X_i) = \begin{cases} +1 & if (X_j - X_i) > 0 \\ 0 & iif (X_j - X_i) = 0 \\ -1 & if (X_j - X_i) < 0 \end{cases}$$

$$VAR(S) = \frac{1}{18}\left[n(n-1)(2n+5) - \sum_{p=1}^{q} t_p(t_p - 1)(2t_p + 5) \right] \tag{6}$$

$$Z = \begin{cases} \dfrac{S-1}{\sqrt{VAR(S)}} & if\ S > 0 \\ 0 & if\ S > 0 \\ \dfrac{S+1}{\sqrt{VAR(S)}} & if\ S < 0 \end{cases}$$

where n is the length of time series; t_p is the number of data points for pth values; q is the number of tied groups in the data

230   set; and $VAR(S)$ is the variance of S. When $VAR(S)>0$, it indicates an upward trend in the precipitation series. When $VAR(S)$

< 0, a negative trend. *Z* value is to detect whether the trend is significant. If $|Z|>Z_{(1-0.5\times\alpha)}$, there exists a statistically significant trend in the series. $Z_{(1-0.5\times\alpha)}$ is the critical value for *p* value of 0.05 from the standard normal table.

Spatial distribution of precipitation hazards is analyzed using a GIS method. Extreme precipitation is the main disaster-causing factor of floods in the study area. The extreme precipitation thresholds of different probabilities are used to evaluate the risk. The number of events above the thresholds are calculated at each meteorological station. The inverse distance weighted method (IDW) is then used to interpolate and zone the number after validation with observations, with the purpose to show the spatial characteristics of the extreme precipitation risk.

3 Results and discussion

3.1 Frequency and contributions of precipitation events

Runs of 12-H precipitation in each station were calculated with records of precipitation >0.1mm. Runs are defined as consecutive precipitation series in this paper. 1-run refers to a precipitation event recorded in 12 hours. 2-run refers to an event with precipitation recorded in two consecutive 12-hour intervals, and so on. If no precipitation is recorded at an interval greater than 12 hours, precipitation is defined as discontinuous and divided into two runs. This definition helps keep the calculated events independent. We further calculated their frequency and contribution to the total precipitation in all stations and plotted them in Figure 2. Figure 2 showed that the frequency of precipitation events decreased with runs increasing. 1-run continuous precipitation event occurred most frequently, accounting for 39.0% of the total events; followed by the 2-run, with a frequency of 21.7%. The frequency of events ≤4 runs accounted for as high as 83.5% of the total events. The frequency of events ≤10 runs reached 98.6%. Events greater than 10 runs only accounted for 1.4% of the total. This indicated that the study area was mainly characterized with short duration precipitation events. Events of 1 to 4 runs occurred most commonly (frequency> 10%). Events greater than 10 runs rarely occurred. The longest consecutive event was the 28-run, which only occurred once at Jgs station in June 1993.

Figure 2 also shows that the contribution of runs of precipitation events to the total precipitation rose slowly first and then fell sharply. Contributions gradually increased from 9.5% to 16.3% from 1-run events to the 3-run. 3-run precipitation events contributed the most to the total precipitation. Contribution of events >14 runs decreased to less than 1%; Cumulative contributions of events with 1-10run counted for 92.6% while events greater than 10 runs counted for only 7.4%. This indicates that continuous precipitation events that contributed the most to total precipitation were events of 1-10 runs. The precipitation events with a longer duration had lower frequency and contributed less to the total precipitation.

Frequency and contribution to total precipitation of all runs in the study area were not proportional according to Figure 2. Frequencies of 1-run and 2-run events were higher than their contribution rates. Contribution rates of events >3 runs were all greater than their frequency. The frequency of the 1-run precipitation event (Its frequency was 39% and contribution was 9.5%) was 2.61 times bigger than that of the 3-run (Its frequency was 14.9% and contribution was 16.3%), but the contribution rate of the former was only 58% of the latter events. This indicated that precipitation events of fewer than 3 runs

occurred most often, but the total amount was small. 3-run precipitation events contributed the most precipitation but with lower frequency and would be key events for flood monitoring.

Figure 3 shows the cumulative probability distribution and fitted gamma curves in stations. Consecutive events with fewer than 10 runs showed an abrupt rainfall rise, up to more than 250mm in all stations. Rainfall of runs longer than 10 roses slowly, with increasing rainfall less than 30mm in most stations. This result showed similar findings to the analysis in Figure 2, that is, precipitation events with very long duration rarely occurred and had minimal contribution to the total. Therefore, 1-10 runs were selected as experimental data for estimating the risk in the follow-up analysis.

3.2 Gamma fits of precipitation events

3.2.1 Estimated distribution of precipitation events

As presented in Section 2.3, the gamma function was used to fit observed precipitation data first with a view to providing smooth changes and long-time projection. Table 3 shows the mean values of α and β of the gamma curves in the four seasons. Related research shows that when the shape parameter α was $\leqslant 1$, the gamma distribution has a asymmetric J-shaped probability density function (Loucks et al., 2005), which indicates that events with small amounts of rainfall account for a substantial large proportion, while events with large amounts of rainfall account for very small proportion (Rodrigo, 2010). This case is common for the four seasons in Table 3, especially in summer and autumn when α is $\leqslant 0.1$, indicating that these two seasons are characterized with occasional and sudden extreme heavy precipitation in all stations. The β parameter characterizes the scale of the gamma distribution. When β increase, the distribution curve squeezes leftward and upward, indicating high intensity of precipitation (Rodrigo, 2010). β has a greater temporal variability. β is the biggest in summer, followed by that in spring, autumn and winter. The highest values of β in spring are from Nd and Ln. These two stations are located in the mountainous upstream areas where northerly cold air meets with warm air from the ocean in spring, often resulting in frontal and cyclone precipitation. The highest values of β in summer appear in Nc, Zs and Yof, which are located in the alluvial plains where the precipitation is often caused by typhoons heading west and southwest in summer (Yin et al., 2007). The highest values of β in autumn are in Sc, Yof, Nd and Ln, indicating that fronts, typhoons and other air activities are frequent in autumn and the main precipitation occurs in the hilly area of the upper Ganjiang river.

3.2.2 Trends of the gamma parameters

Temporal trends of the shape parameter α and the scale parameter β were further analyzed using the Mann–Kendall. Table 4 summarizes the results, which indicated that precipitation would occur more occasionally but with higher intensity in spring, winter and autumn. The two parameters in most stations are experiencing more intensive changes in spring. α in spring shows a significant downward trend in Yf, Yc, Jgs, Sc, Nc, Zs and Nd with the absolute value of Z bigger than 2.32 while β exhibits an upward trend in Yf, Lh, Zs, Nd and Ln. The trend of α is tested downward in Jgs, Yof and Ln in autumn while the trend of β is upward in Ja, Zs and Yof. β in Ja, Jgs, Sc, Gx, Yof and Nd in winter. No obvious trends are detected in

summer. Studies have showed that decreasing the shape parameter α will reduce the threshold for the extreme precipitation threshold, which in turn increases the risk of storm flooding (Rodrigo, 2010). The down-trend α along with upward-trend scale parameter β in Yf, Zs, Nd means that the intensity and occasional probability of concentrated precipitation events in these stations will increase in the future, which will thereby increase the risk of storm floods in spring. Similar cases were also found in Yof in autumn and Jgs in winter, which indicated that extreme precipitation would become more intensive with a warmer and warmer climate. The particular case is the station of Jgs, with α decreasing in all the seasons except summer. Jgs is located in the mountain at an elevation of 843m. We may infer this mountainous station will present increasingly obvious maritime precipitation characteristics in the future.

3.3 Risk of extreme precipitation

3.3.1 Estimation of thresholds for extreme precipitation

As defined in Section 2.2, the 99% percentile of the 12-H precipitation data and their gamma distribution estimates were first calculated as extreme precipitation thresholds. Table 5 shows the mean values for each station. The estimated threshold values show higher variability from winters to summers in Table 5. The maximum threshold values occur in summer, followed by spring, autumn and winter. The study area is mainly controlled by monsoons and typhoons in summer, which result in the most concentrated heavy precipitation (Shan et al., 2001). In spring, the ridge of the subtropical high system moved to the south of 20°N latitude. The warm and humid air from the south along the subtropical high ridge intersects with cold air from the north, forming fronts and cyclones activities which bring a wide range of cloudy and rainy weather. Autumn and winter are often affected by the winter monsoon, which is characterized with cold air and low precipitation (Zhang and Song, 2018).

What stands out in Table 5 is that the estimated gamma values are 0.3-0.8% lower than those observed on average, with the smallest in spring (0.3%) and the largest in autumn (0.8%). This result is similar to that in the literature of Rodrigo (Rodrigo 2010). A slightly lower threshold for extreme precipitation will increase the estimated risk, which allows risk managers to improve risk management before storm floods occur. Therefore, the lower values from the Gamma function would help reduce risks. The 99th percentile estimates are maintained as the threshold values to obtain the risk analysis.

The estimated thresholds of 12 hours to 120 hours' precipitation events (1 to 10 runs of 12-H events) were also calculated and plotted. The Kolmogorov–Smirnov test (KS) was used to test the goodness of the fits at the 95% confidence level. KS values range from 0.06 to 0.12, which show that Gamma distribution had a good agreement with the selected thresholds from the observations. Forty-eight fits (4 seasons × 12 stations) were calculated eventually and Figure 4 shows an example in Gx. Its horizontal axis represents scenarios or probability while the vertical axis represents tthresholds of extreme precipitation events in millimeters (mm). The lowest curve is fitted from 1-run observed precipitation. Curves from the 2-run to the 10-run are higher and higher. Figure 4 shows that there are bigger intervals between curves in summer and winter, indicating that runs of precipitation events in summer and winter have a greater impact on the extreme event thresholds.

Compared with 5 to 10 runs, the intervals are even bigger between 1-4 runs, indicating that the precipitation threshold changes greatly when the events happen within 48 hours. The curve slopes in all the four pictures are steep when the probability is less than 0.5 (1/2), which shows precipitation thresholds increase quickly. The slopes gradually decline when the probability is less than 0.2 (1/5). It shows the precipitation threshold increases slowly as the probability decreases. Fits in other stations show similar trends.

With the help of these gamma fits, thresholds under any given probability can be estimated. The orange hollow points in Figure 4 show estimates when the return period is set to be one in 2 years (its probability is 0.5), one in 5 years (0.2), one in 10 years (0.1), one in 20 years (0.05) and one in 50 years (0.02) respectively, which will be used for risk analysis later in the following section.

3.3.2 Extreme events and floods

The estimated thresholds in Section 3.3.1 could help to analyze extreme precipitation events and their risks. In order to identify what kinds of extreme events would cause floods, we selected Gx, a meteorological station, and Hanlinqiao, a hydrological observation station to do a comparative analysis, due to the available hydrological data. Figure 5 shows their location. Gx (E115°, N25.87), located at the lower reach of the Gongshui River (a branch of the Ganjiang River in its upper reach), is a national meteorological observatory. It is one of the four national basic stations in the upper reach of the Ganjiang River. The records in Gx began in 1951 and they are relatively complete with good data consistency. Hanlinqiao is a regional representative hydrological station at E115°12′ and N26°03′. It was established in February 1953 and is located in Laoheshi Village, Jibu Town, Ganxian County, downstream of the Pingjiang River, whose catchment area is 2689 km^2. It is 17 kilometres away from the entrance to The Gongshui River. The two stations are close, and the representative area covers almost the same region.

The extreme events supposed to be with risk causing floods in Gx are selected according to the following standards and Table 6 shows the number of selected events:

1) Events above thresholds estimated by the Gamma curves of 1-10 runs in Section 3.3.1;

2) Events under the scenarios of probability at 0.5, 0.2, 0.1, 0.05 and 0.02, representing return periods of 2, 5, 10, 20 and 50 years respectively.

3) The time intervals between two events are greater than one run (12 hours).

4) Events between 2009-2014, which is the period of the available hydrological data at Hanlinqiao station.

The flood events in Hanlinqiao is selected according to the standards below and Table 7 shows the result:

1) Events above the threshold, which is the 99% percentile of the daily flow records

2) The time interval between two events greater than one day, that is, the estimated convergence time from the farthest point to the outlet in the catchment.

Analysis from Tables 6 and 7 shows that the predicted extreme precipitation events have similar trends as the flood records. Both of them have more events in spring than in summer, followed by autumn and winter. Table 6 shows the predicted

events of all the runs in spring account for more than 40 percent under the scenarios of probability at 0.5, 0.2, 0.1, and about 30 percent under scenarios of probability at 0.05 and 0.02. Events in summer account for more than 30 percent under all the scenarios. Those in autumn and winter only account for 20% or so from 2009 to 2014. Records in Hanlinqiao find 12 flood events in the 6 years. Seven events were in spring and five in summer. No events are found in autumn and winter. The precipitation records at Gx were selected with the flood occurrence date. There are 9 precipitation events found on the same day when the floods happened, with the highest precipitation of 72.2mm in 12 hours and 118.1mm in 24 hours.There was no precipitation recorded with the same date of the rest three floods, but precipitations were found on the previous day, which the highest precipitation of 73.3 mm in 12 hours before the date and 83 mm in 24 hours before the date. Two floods were found with a 6-run precipitation event in the early stage, four floods with a 4-run precipitation event, two floods with a 3-run precipitation event, one flood with a 2-run precipitation event, and three floods with a 1-run precipitation event. Compared with the flood records, thresholds in Scenario 1 (probability at 0.5) are a little lower, which will overestimate the number of extreme precipitation events. Scenarios 3, 4 and 5 (probabilities at 0.1, 0.05 and 0.02) have high thresholds which will underestimate the number of the flood events. The predicted extreme precipitation events from Scenario 2 (probability at 0.2) are very close to the recorded flood events.

Of all the runs under Scenario 2, the predicted events from runs more than 7 are lower than the recorded floods. It is a complex process from precipitation to floods, involving several disaster-generating environments such as land covers, topography, soil, temperature, shape of the catchment area, etc. It is reasonable that the predicted extreme precipitation events are bigger than or equal to flood events in the risk assessment. Therefore, runs 1, 2, 3, 4, 5 and 6 are more suitable for predicting extreme events. According to the flood events at Hanlinqiao Station, the predicted events from Run 1 (one 12-H precipitation) under Scenario 1 are almost double the flood records. Events from Runs 2,3,4,5 and 6 are all more or very close to the flood records. The analysis indicates that events predicted with the gamma distribution from precipitation of 12-72 hours are all very helpful for flood estimates, while those from more than 72 hours, which will low estimate the flooding risk. There are some cases where small precipitation (small than the given threshold) was observed at the beginning, which was not considered to cause floods. However, a new record of precipitation that was just above the threshold in the following periods eventually led to flooding because of rainfall accumulated in the previous period. If time intervals of precipitation are too long, this flood event will be missed because of the high threshold. Run 1(12-H precipitation) will be the best time interval for predicting extreme events in disaster management, which will avoid such missed cases.

3.3.3 Spatial distribution of extreme precipitation risk

The paper further analyzed the spatial distribution of extreme precipitation risk in the study area. The method is listed below according to the analysis above.

1) The observed precipitation was 12-H precipitation from the 12 meteorological stations. The 99th percentile was selected as thresholds in each season.

2) A gamma function was used to fit the observed data. Thresholds were calculated at a given probability of 0.2 from the gamma curves according to Section 3.3.2. Events bigger than the threshold were considered as the extreme precipitation events and was calculated for risk map.

3) The number of events in all station was further interpolated with an inverse distance method. The results were mapped and stretched from low to high, according to the number of events.

Maps of extreme precipitation risk in spring, summer, autumn and summer with the methods above are followed in Figure 6 to show spatial distribution of extreme precipitation risk. Figure 6 shows that the high-risk centers of extreme precipitation are distributed on the east side of the Luoxiao Mountains in spring, moving south to the upper reaches of the Ganjiang River, which is the north side of the Nanling Ranges in summer. Two new high-risk centers are found in the middle reaches of the Ganjiang River, near the west side of Wuyi Mountain in autumn and tend to move eastward and northward in winter. The low-risk areas are distributed in the Jitai Basin, which is in the middle reaches of the Ganjiang River and the upper Ganzhou Basin in spring, moving north to the lower reaches to the Poyanghu Lake in summer, then moving slightly to the south in autumn. In winter, a new low-risk center is formed in the northwest, and move to the northwest and the northwest near the Luoxiao Mountain in the west. In general, extreme precipitation has a high risk of flooding in the upper reaches of the Ganjiang River, the Jitai Basin in the middle reaches and the northern plains. Risk tends to increase with elevation in the northern river-lake plain area and the Jitai Basin in the midstream area while risk in the southern hilly area is the opposite, shows signs of decreasing as elevation rises. This risk result is similar to the conclusions of the literature of Yin et al.(Yin et al., 2018).

The main weather systems that cause extreme precipitation in the study area include low- and medium-level shear lines, low-level jets, typhoon with low pressure, etc (Shan et al., 2001). Monsoons in spring and summer from the tropical ocean cyclones run southwest in the study area, are uplifted with micro-topography and result in high-risk centers in the west and south mountain regions. The winter monsoons in autumn and winter from deep inland move south-eastward and form frontal precipitation when they encounter stranded warm air currents, causing high-risk centers in the eastern and southern parts of the study area.

3.4 Discussion

3.4.1 Time scales of precipitation

Precipitation events, especially occasional extreme precipitation events, is highly variable in time (Beck et al., 2015) and intermittency is a core characteristic (Trenberth et al., 2017). This paper investigated the time scales of precipitation with 12-H data and found 3-run precipitation events contributed the most precipitation but with lower frequency. The study area was mainly characterized with short-duration precipitation events, and events greater than 10 runs occurred very rarely. Hence, short duration precipitation events would be a key hazard factor for extreme precipitation forecasting, flood and disaster risk management analysis. Section 3.2 further analyzed the trend of short duration precipitation and found that it

would occur more occasionally but with higher intensity in future. Other associated studies have yielded similar results. Cheng et al. investigated the precipitation Intensity-Duration-Frequency (IDF) in a changing climate and found that climate-induced changes on heavy rainfall events are non-uniform. The shorter precipitation events have changed more in the past decades, while longer events have not changed substantially (Cheng and Aghakouchak, 2014). Hosseinzadehtalaei et al. found the frequency of sub-daily extreme precipitation events of 50- and 100-year return periods will be tripled under the high-end RCP8.5 scenario in the future climate change, which will increase the risk of flooding (Hosseinzadehtalaei et al., 2020). Similar cases are also found in China. Ren et al. analyzed the data from 2,300 stations across China. Their research shows that the frequency of trace precipitation (precipitation with a daily rainfall of less than 0.1 mm) has shown a more significant downward trend than the frequency of light rain events in the eastern monsoon region. The frequency of light precipitation in the eastern monsoon region has shown a very obvious downward trend (Ren et al., 2016). The Ganjiang river basin is located in the south of the east Asian monsoon region. Changes in short-duration precipitation events caused by climate warming will cause a higher risk of flooding, which is certainly the key indicator for further study on climate change, floods and other extreme weather disasters.

3.4.2 Extreme precipitation risk

In fact, most precipitation events bring us necessary beneficial freshwater resources. Only a few events, especially extreme precipitation events, cause disasters and losses. However, what extreme events will result in flooding is not very clear. Researchers should consider how extreme precipitation is defined and carefully choose the data for their analysis of extreme precipitation (Pendergrass, 2018). We compared the extreme precipitation events from 1-10 runs of 12-H data with the flood records at the hydrological observation station and found that the number of events from 1, 2, 3 and 4 runs were close to the number of flood records. The number of diagnosed extreme events decreases as precipitation runs of 12-H increase, i.e, precipitation of more than 5 runs would low estimate the risk. Similar case has also been found in the literature of Merino et al. (Merino, Fernández-González et al. 2018), who selected 29 floods between 2000 and 2014 in Spain and compared them with the extreme precipitation events calculated with hourly and daily precipitation data in order to find their capability to identify flood events. The result shows that no extreme precipitation events are identified in eight of the flood events using definition based on daily precipitation, but events based on sub-daily data permit much more accurate identification of events posing hydrologic risks (Merino et al., 2018). Obviously, it would be better to use short-duration data, for example, sub-daily precipitation, in extreme event analysis to avoid underestimation of potentially dramatic consequences they caused, such as flooding. In practice, daily precipitation series are commonly used to analyze extreme precipitation events with sufficient quantities and little homogeneity problems. The reason might be that high-time resolution precipitation data are not provided or recorded in most regions. Therefore, remotely sensed data from satellites or rain radar would be used to replace sub-daily precipitation in follow-up research (Müller and Kaspar, 2014).

4 Conclusion

455 In this study, we investigated the frequency and contributions of precipitation events using sub-daily records in meteorological stations in the Ganjiang river basin; identified their changes and time scales using gamma distribution and M-K test; and explored the definition, thresholds of extreme precipitation events and flooding risk. We further spatially mapped the extreme precipitation risk across the entire study area and analyzed the distribution characteristics. Based on the analysis presented in this study, the following conclusions can be drawn:

460 (1) For frequency and contributions, it was found events of 1 to 4 runs occurred most commonly and events of 1-10 runs contributed the most to the total precipitation. The frequency of events ≤4 runs accounted for as high as 83.5% of the total events. Events greater than 10 runs only accounted for 1.4% of the total. The cumulative contributions of events with 1-10 run counted for 92.6% while events greater than 10 runs counted for only 7.4%. 3-run precipitation events contributed the most precipitation but with lower frequency, which would be key events for flood monitoring.

465 (2) The gamma parameters analysis shows that extreme precipitation has the characteristics of high intensity and occasional occurrence in summer in all stations. In summer, the shape parameter α is ≤0.1 and the scale parameter β is the highest. The highest β values indicate that stations in mountainous areas and the transition areas from mountains to plains, such as Ningdu, Longnan Nanchang, Zhangshu and Yongfeng, are characterized with high-intensity precipitation in spring. Suichuan, Yongfeng, Ningdu and Longnan often have high-intensity precipitation in autumn. Temporal trends analysis of α and β

470 shows the intensity and occasional probability of precipitation events will increase in spring in the future in Yifeng, Zhangshu and Ningdu, which will in turn increase the risk of storm floods.

(3) Extreme precipitation risk shows the risk increasing as elevation increases in the northern river-lake plain area and the Jitai Basin in the midstream area, while the risk in the southern hilly area is the opposite, decreasing with elevation. Elevation and weather systems such as medium-to-low--level shear lines, low-level jet, and the southward typhoons are the

475 key disaster-pregnant factors for disaster management.

Author contribution: Liu Guangxu and Wan Zhiwei designed the structures and prepared the manuscript. Xiang Aicun and Lin Sichen collected and processed data. Zhou Yang, Wu Jie and Wang Yuandong revised and improved the manuscript.

Competing interests: The authors declare that they have no conflicts of interest.

Acknowledgements: We would like to thank the funding from the Social science Planning project of Jiangxi Province

480 (19GL30), Humanities and Social Science Research Planning Project for Universities of Jiangxi Province (No. GL20116), Science and Technology Project of Jiangxi Department of Education (No. GL20116) and the Natural Science Foundation of China (NSFC) (No. 42161019).

Reference

Ahmad, I., Tang, D., Wang, T., Wang, M., and Wagan, B.: Precipitation trends over time using Mann-Kendall and spearman's rho tests in swat river basin, Pakistan, Advances in Meteorology, 2015.

Asadieh, B., Krakauer, N., and Y.: Global trends in extreme precipitation: climate models versus observations, Hydrology & Earth System Sciences, 2015.

Bao, J., Sherwood, S. C., Alexander, L. V., and Evans, J. P.: Future increases in extreme precipitation exceed observed scaling rates, Nature Climate Change, 7, 128-132, 2017.

Beck, F., Bárdossy, A., Seidel, J., Müller, T., Sanchis, E. F., and Hauser, A.: Statistical analysis of sub-daily precipitation extremes in Singapore, Journal of Hydrology: Regional Studies, 3, 337-358, 2015.

Chen, M.: Research on the Prevention and Control of Urban Rainstorm and Flood Disasters Based on the Construction of Standardization System (in Chinese), Opportunities for Standardization Reform and Development-The 12th China Standardization Forum, Hanzhou2015.

Cheng, L. and AghaKouchak, A.: Nonstationary precipitation intensity-duration-frequency curves for infrastructure design in a changing climate, Scientific reports, 4, 1-6, 2014.

Easterling, D. R., Alexander, L. V., Mokssit, A., and Detemmerman, V.: CCI/CLIVAR workshop to develop priority climate indices, Bulletin of the American Meteorological Society, 84, 1403-1407, 2003.

Easterling, D. R., Meehl, G. A., Parmesan, C., Changnon, S. A., Karl, T. R., and Mearns, L. O.: Climate extremes: observations, modeling, and impacts, Science, 289, 2068-2074, 2000.

El Adlouni, S. and Ouarda, T.: Frequency analysis of extreme rainfall events, Rainfall: State of the science, 191, 171-188, 2010.

Fischer, E. M., Beyerle, U., and Knutti, R.: Robust spatially aggregated projections of climate extremes, Nature Climate Change, 3, 1033-1038, 2013.

Gao, T. and Xie, L. a.: Study on progress of the trends and physical causes of extreme precipitation in China during the last 50 years (in Chinese), Advances in Earth Science, 29, 577, 2014.

Gao, T., Wang, H. J., and Zhou, T.: Changes of extreme precipitation and nonlinear influence of climate variables over monsoon region in China, Atmospheric research, 197, 379-389, 2017.

Haylock, M. and Nicholls, N.: Trends in extreme rainfall indices for an updated high quality data set for Australia, 1910–1998, International Journal of Climatology: A Journal of the Royal Meteorological Society, 20, 1533-1541, 2000.

Hosking, J. R.: L-moments: Analysis and estimation of distributions using linear combinations of order statistics, Journal of the Royal Statistical Society: Series B (Methodological), 52, 105-124, 1990.

Hosseinzadehtalaei, P., Tabari, H., and Willems, P.: Climate change impact on short-duration extreme precipitation and intensity–duration–frequency curves over Europe, Journal of hydrology, 590, 125249, 2020.

Hu, Q., Yang, D., Wang, Y., and Yang, H.: Accuracy and spatio-temporal variation of high resolution satellite rainfall estimate over the Ganjiang River Basin, Science China Technological Sciences, 56, 853-865, 2013.

Kliche, D. V., Smith, P. L., and Johnson, R. W.: L-moment estimators as applied to gamma drop size distributions, Journal of applied meteorology and climatology, 47, 3117-3130, 2008.

Li, J., Zhang, L., Tian, W., Guo, P., and Dong, Q.: Risk-based Study of Flood Frequency Standard for Highway Subgrade (in Chinese), China Journal of Highway and Transport, 27, 32-38, 2014.

Li, N., Tang, G., Zhao, P., Hong, Y., Gou, Y., and Yang, K.: Statistical assessment and hydrological utility of the latest multi-satellite precipitation analysis IMERG in Ganjiang River basin, Atmospheric research, 183, 212-223, 2017.

LIU, X., FAN, S., WANG, J., and XU, C.: Analysis on Meteorological Characteristics of a Strong Storm Disasters in the Eastern Foot of Longmen Mountain, Journal of Catastrophology, 33, 2018.

Loucks, D. P., Van Beek, E., Stedinger, J. R., Dijkman, J. P. M., and Villars, M. T.: Water Resources Systems Planning and Management: An Introduction to Methods, Models and Applications, Springer International Publishing, 2005.

Müller, M. and Kaspar, M.: Event-adjusted evaluation of weather and climate extremes, Natural Hazards and Earth System Sciences, 14, 473-483, 2014.

Merino, A., Fernández-González, S., García-Ortega, E., Sánchez, J., López, L., and Gascón, E.: Temporal continuity of extreme precipitation events using sub-daily precipitation: application to floods in the Ebro basin, northeastern Spain, International Journal of Climatology, 38, 1877-1892, 2018.

Mukherjee, S., Aadhar, S., Stone, D., and Mishra, V.: Increase in extreme precipitation events under anthropogenic warming in India, Weather and climate extremes, 20, 45-53, 2018.

O'Gorman, Paul, A., Schneider, and Tapio: The physical basis for increases in precipitation extremes in simulations of 21st-century climate change, Proceedings of the National Academy of Sciences of the United States of America, 2009.

535

Pachauri, R. K., Allen, M. R., Barros, V. R., Broome, J., Cramer, W., Christ, R., Church, J. A., Clarke, L., Dahe, Q., and Dasgupta, P.: Climate change 2014: synthesis report. Contribution of Working Groups I, II and III to the fifth assessment report of the Intergovernmental Panel on Climate Change, IPCC, Geneva,Switzerland, 151 pp.2014.

Papalexiou, S., Koutsoyiannis, D., and Makropoulos, C.: How extreme is extreme? An assessment of daily rainfall distribution tails, Hydrology and Earth System Sciences, 17, 851-862, 2013.

540

Pendergrass, A. G.: What precipitation is extreme?, Science, 360, 1072-1073, 2018.

Pendergrass, A. G. and Hartmann, D. L.: Changes in the Distribution of Rain Frequency and Intensity in Response to Global Warming*, Journal of Climate, 27, 8372-8383, 2014.

Pfahl, S., O'Gorman, P. A., and Fischer, E. M.: Understanding the regional pattern of projected future changes in extreme precipitation, Nature Climate Change, 7, 423-427, 2017.

545

REN, G., LIU, Y., SUN, X., ZHANG, L., Yuyu, R., Ying, X., Hua, Z., Yunjian, Z., Tao, W., and Yanjun, G.: Spatial and temporal patterns of precipitation variability over mainland China: III : causes for recent trends, Advances in Water Science, 27, 327-348, 2016.

Ren, Z., Zhang, M., Wang, S., Zhu, X., Dong, L., and Qiang, F.: Changes in precipitation extremes in South China during

550

1961-2011 (in Chinese), Acta Geographica Sinica, 69, 640-649, 2014.

Rodrigo, F.: Changes in the probability of extreme daily precipitation observed from 1951 to 2002 in the Iberian Peninsula, International Journal of Climatology, 30, 1512-1525, 2010.

Saidi, H., Ciampittiello, M., Dresti, C., and Ghiglieri, G.: Assessment of trends in extreme precipitation events: a case study in Piedmont (North-West Italy), Water Resources Management, 29, 63-80, 2015.

555

ŞEN, Z. and Eljadid, A. G.: Rainfall distribution function for Libya and rainfall prediction, Hydrological sciences journal, 44, 665-680, 1999.

Shan, J., Zhang, Y., and Zhang, Y.: Features analysis about weather system to five river basins of Jiangxi province and important precipitation procedure, JIANGXI METEOROLOGICAL SCIENCE & TECHNOLOGY, 14-18, 2001.

ShI, P., Kong, F., and Fang, J.: Spatio-temporal Patterns of China Decadal Storm Rainfall (in Chinese), Scientia Geographica

560

Sinica, 34, 1281-1290, 2014.

Sillmann, J., Kharin, V. V., and Zhang, X. B.: Climate extremes indices in the CMIP5 multi-model ensemble: Part 1, Journal of Geophysical Research Atmospheres, 118, 1-18, 2013.

Soro, G. E., Noufé, D., Goula Bi, T. A., and Shorohou, B.: Trend analysis for extreme rainfall at sub-daily and daily timescales in Côte d'Ivoire, Climate, 4, 37-52, 2016.

565

Sun, Y. and Stein, M. L.: A stochastic space-time model for intermittent precipitation occurrences, The Annals of Applied Statistics, 9, 2110-2132, 2015.

Tabari, H.: Climate change impact on flood and extreme precipitation increases with water availability, Scientific reports, 10, 1-10, 2020.

Tabari, H. and Willems, P.: Lagged influence of Atlantic and Pacific climate patterns on European extreme precipitation,

570

Scientific reports, 8, 1-10, 2018.

Talchabhadel, R., Karki, R., Thapa, B. R., Maharjan, M., and Parajuli, B.: Spatio - temporal variability of extreme precipitation in Nepal, International Journal of Climatology, 38, 4296-4313, 2018.

Trenberth, K. E.: Conceptual framework for changes of extremes of the hydrological cycle with climate change, in: Weather and climate extremes, Springer, 327-339, 1999.

575

Trenberth, K. E., Zhang, Y., and Gehne, M.: Intermittency in precipitation: Duration, frequency, intensity, and amounts using hourly data, Journal of Hydrometeorology, 18, 1393-1412, 2017.

Trenberth, K. E., Dai, A., Rasmussen, R. M., and Parsons, D. B.: The changing character of precipitation, Bulletin of the American Meteorological Society, 84, 1205-1218, 2003.

Vivekanandan, N.: Flood frequency analysis using method of moments and L-moments of probability distributions, Cogent

580

engineering, 2, 1018704, 2015.

Wang, Q.: Direct sample estimators of L moments, Water resources research, 32, 3617-3619, 1996.

Wang, X. L.: Accounting for autocorrelation in detecting mean shifts in climate data series using the penalized maximal t or F test, Journal of applied meteorology and climatology, 47, 2423-2444, 2008.

Wang, X. L., Chen, H., Wu, Y., Feng, Y., and Pu, Q.: New techniques for the detection and adjustment of shifts in daily precipitation data series, Journal of applied meteorology and climatology, 49, 2416-2436, 2010.

Westra, S., Alexander, L. V., and Zwiers, F. W.: Global Increasing Trends in Annual Maximum Daily Precipitation, Journal of Climate, 26, 7834, 2013.

Wu, J., Zhou, B., and Xu, Y.: RESPONSE OF PRECIPITATION AND ITS EXTREMES OVER CHINA TO WARMING: CMIP5 SIMULATION AND PROJECTION (in Chinese), Chinese Journal of Geophysics, 58, 3048-3060, 2015.

Wu, X., Guo, S., Yin, J., Yang, G., Zhong, Y., and Liu, D.: On the event-based extreme precipitation across China: Time distribution patterns, trends, and return levels, Journal of hydrology, 562, 305-317, 2018.

Xiao, C., Wu, P., Zhang, L., and Song, L.: Robust increase in extreme summer rainfall intensity during the past four decades observed in China, Scientific reports, 6, 1-9, 2016.

Xu, K., Ma, C., Lian, J., and Bin, L.: Joint probability analysis of extreme precipitation and storm tide in a coastal city under changing environment, PLoS One, 9, e109341, 2014.

Yin, J., Kim, M., Feng, K., and Chen, J.: Comparative Analysis of Three Typhoons Hitting Jiangxi on Routes and Mechanisms of Heavy Rainfall, METEOROLOGY AND DISASTER REDUCTION RESEARCH, 30, 18-22, 2007.

YIN, Z. e., TIAN, P., and CHI, X.: Multi-scenario-based risk analysis of precipitation extremes in China during the past 60 years (1951-2011) (in Chinese), Acta Geographica Sinica, 73, 405-413, 2018.

Zeng, Y. and Lu, E.: Changes of Summer Rainfall and Extreme Precipitation During 1961-2010 in China (in Chinese), Climate Change Research, 11, 79-85, 2015.

Zhang, D. and Song, W.: Northern Hemisphere Atmospheric Circulation Characteristics in 2017/2018 Winter and Its Impact on Weather and Climate in China, Meteorological Monthly, 44, 969-976, 2018.

Zhao, Y., Xiao, D., and Bai, H.: Projection and Application for Future Climate in China by CMIP5 Climate Model (in Chinese), Meteorological Science and Technology, 47, 608-621, 2019.
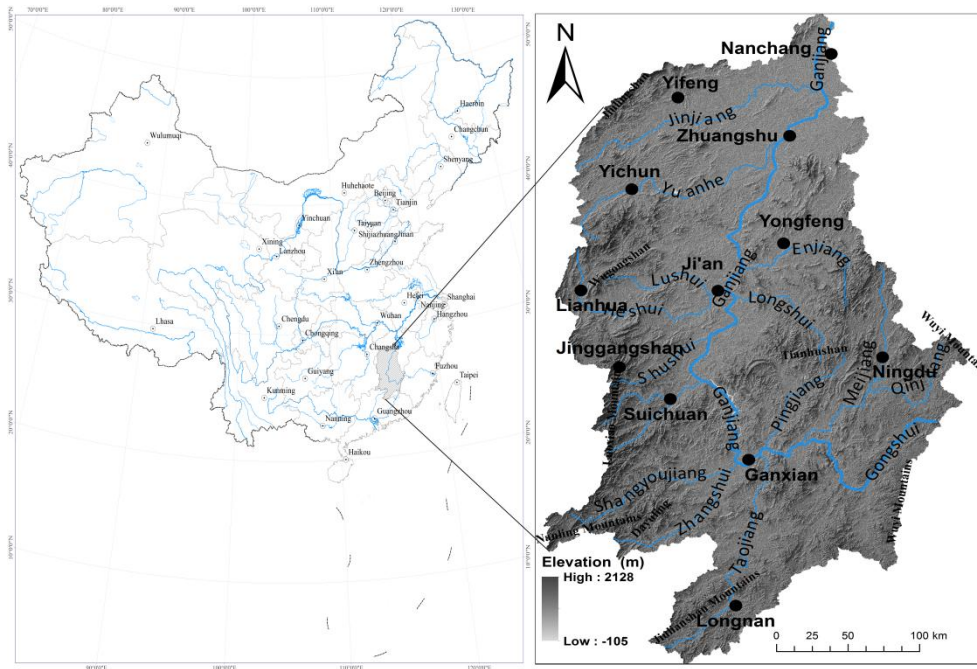
Figure 1 Study area and location of meteorological stations
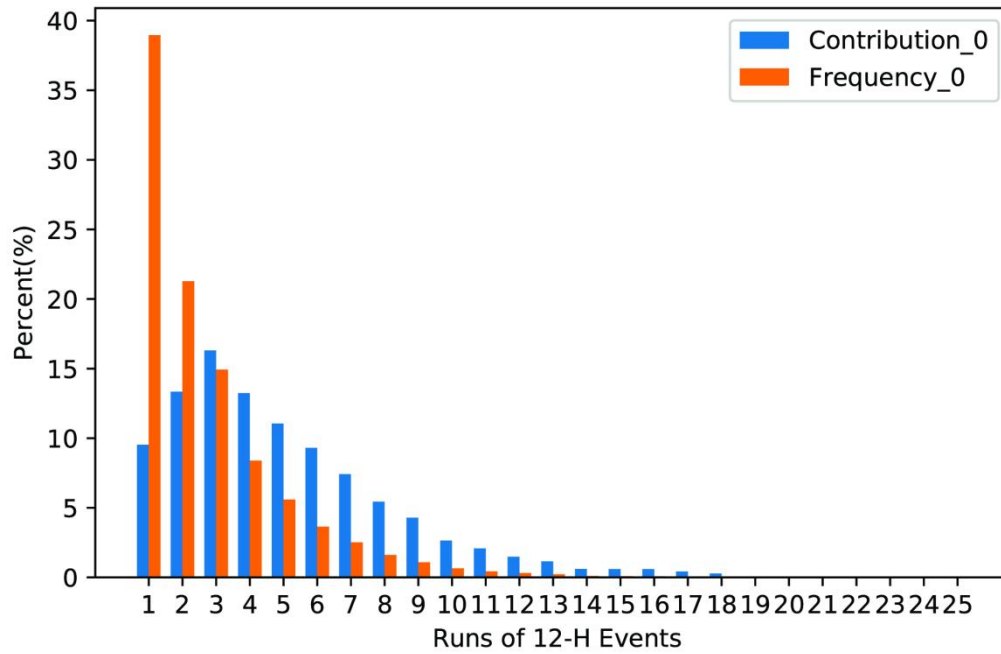
610

Figure 2 Frequency and contribution of runs of 12-H events
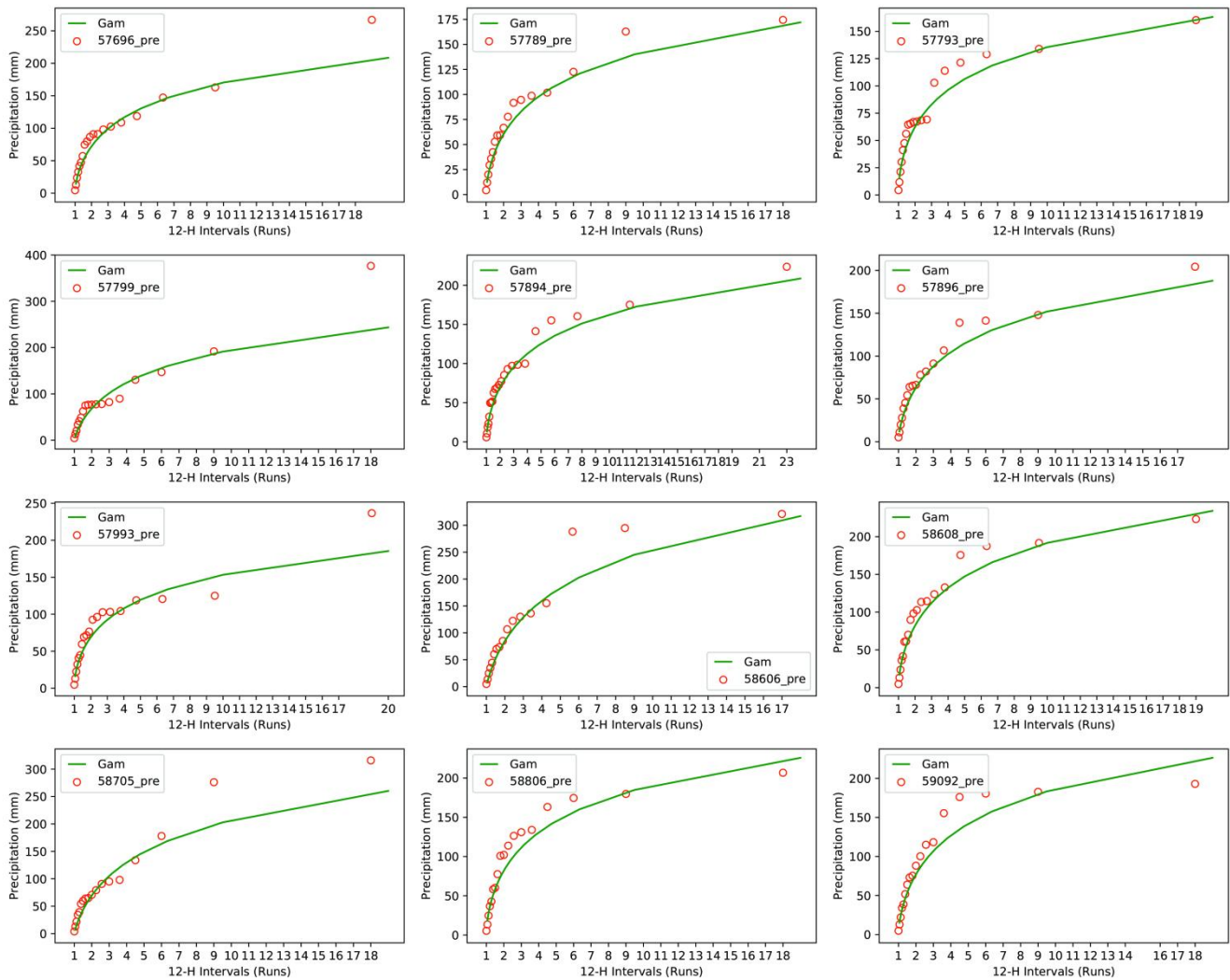
Figure 3 Cumulative precipitation of runs of events. The orange hollow points show observed precipitation events. The green lines represent their gamma estimates
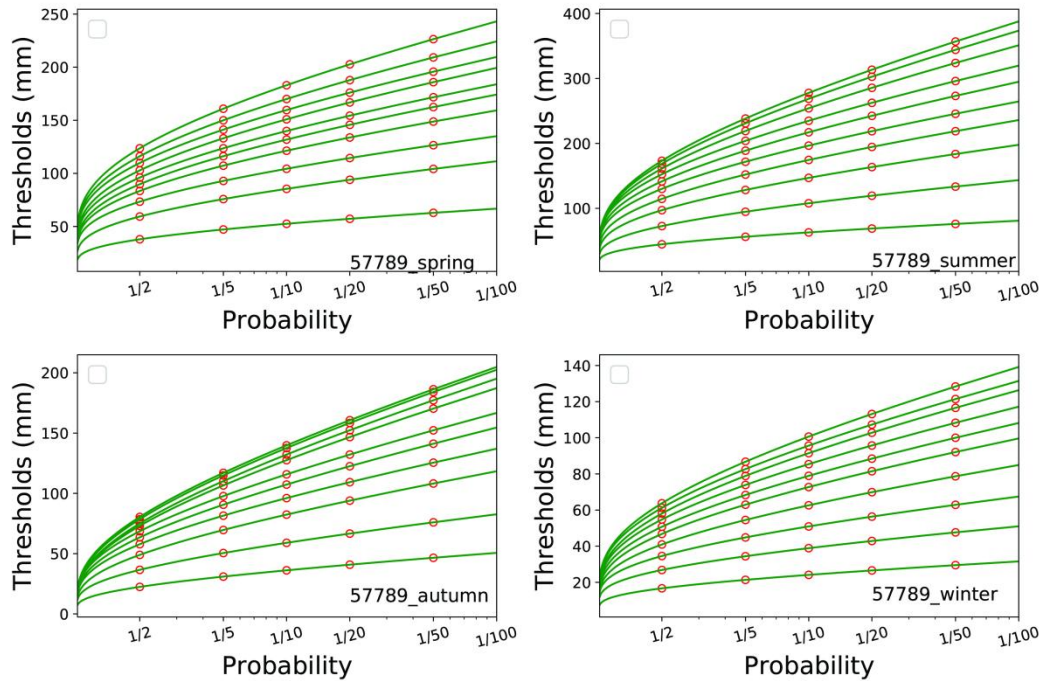
615

Figure 4 An example of extreme precipitation threshold distribution from the gamma fits of 1-10 run 12-H data in seasons. The green lines from bottom to up show the gamma fits of 1-10 runs respectively. The orange hollow points are thresholds calculated with a probability of 0.5 (1/2), 0.2 (1/5), 0.1 (1/10), 0.05 (1/20) and 0.02 (1/50).
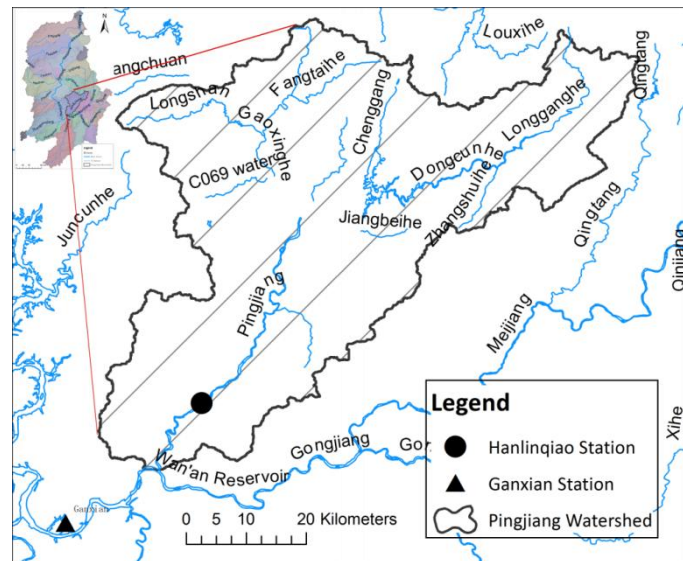
620   **Figure 5 Location of Ganxian meteorological station and Hanlinqiao hydrological observation station**
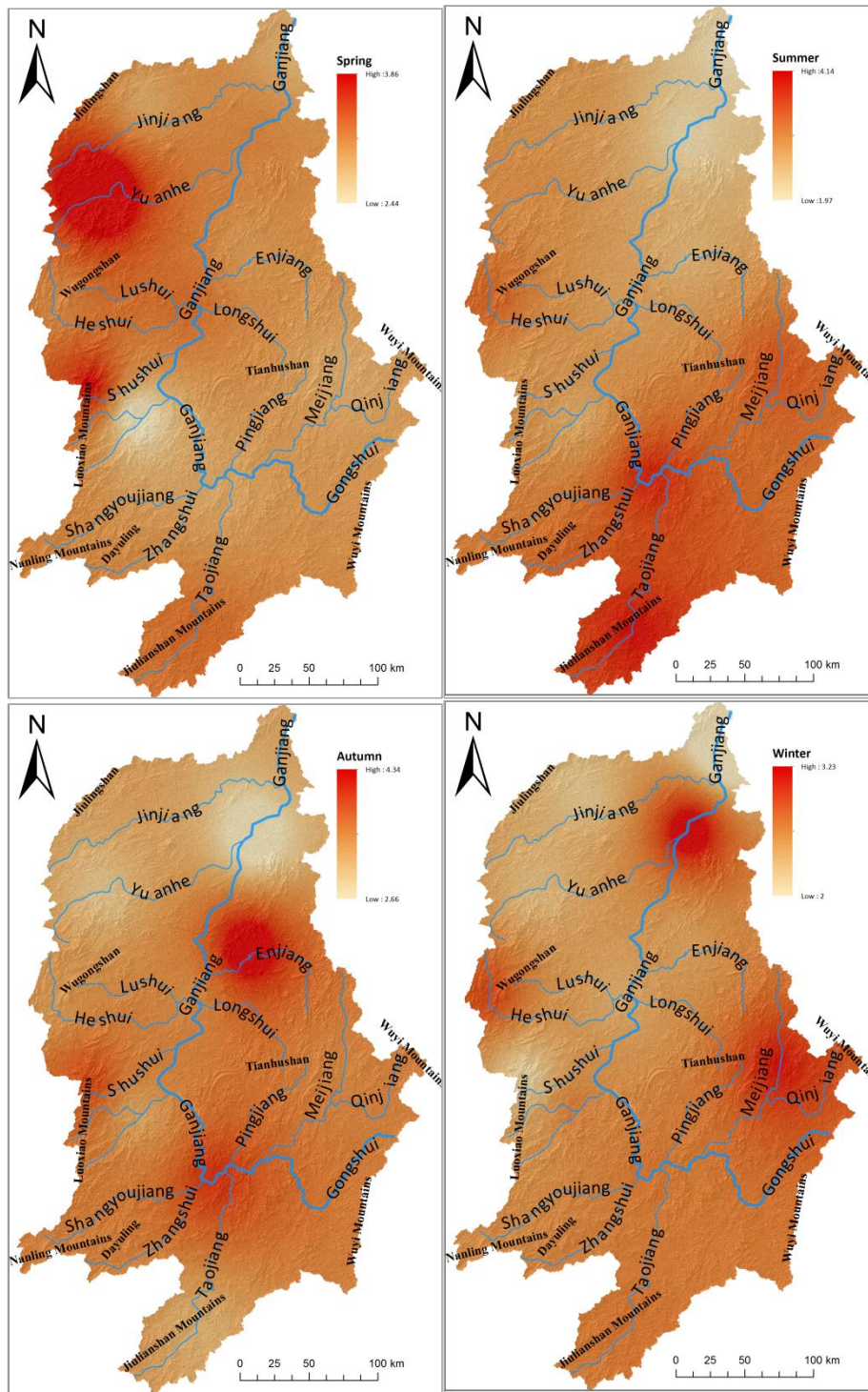
Figure 6 Extreme precipitation risk under Scenario 2 in spring, summer, autumn and winter in the Ganjiang River basin. The colors range from light orange to red, indicating the increasing risk from low to high. The numbers are annual average of the estimated extreme precipitation events.

Table 1 Characteristics of the selected meteorological stations

| Stations | Station Code | Location | | Elevation (m a.s.l) | Observation period (Year) |
		Latitude (N)	Longitude (E)		
Nanchang (Nc)	58806	28.60	115.92	47	1956-2016
Yifeng (Yf)	58806	28.40	114.78	92	1951-2016
Zhangshu (Zs)	58608	28.07	115.55	30	1951-2016
Yichun (Yc)	57793	27.80	114.38	131	1956-2016
Yongfeng (Yof)	58705	27.33	115.42	86	1959-2016
Lianhua (Lh)	57789	27.13	113.95	195	1951-2016
Ji'an (Ja)	57799	27.05	114.92	71	1956-2016
Jinggangshan (Jgs)	57894	26.58	114.17	843	1959-2016
Ningdu (Nd)	58806	26.48	116.02	209	1952-2016
Suichuan (Sc)	57896	26.33	114.50	126	1957-2016
Ganxian (Gx)	57896	25.87	115.00	138	1958-2016
Longnan (Ln)	59092	24.87	114.80	250	1951-2016

630 **Table 2 Seasonal and annual mean precipitation in stations (mm). The data are based on the selected period 1959-2016.**

station	spring	summer	autumn	winter	annual
Yf	667.1	588.2	252.9	249.2	1757.4
Lh	627.4	512.8	228.8	236.7	1605.6
Yc	624.4	522.3	242.2	237.9	1626.8
Ja	604.5	490.2	221.3	211.3	1527.4
Jgs	578.4	774.5	336.4	207.9	1897.2
Sc	494.6	501	273.9	188.2	1457.6
Gx	570.2	458.4	208	209.2	1445.9
Nc	626	556	196.5	214.7	1593.4
Zs	665.4	542.6	215.5	243.7	1667.2
Yof	656.1	550.5	227.3	234.7	1668.6
Nd	706.9	614.7	234.5	224.8	1781
Ln	597.6	544.4	205	196.5	1543.5

Table 3 Mean parameters α (shape) and β (scale, mm/12-H) for gamma distribution in stations

Stations	spring α	spring β	summer α	summer β	autumn α	autumn β	winter α	winter β
Yf	0.1	23.4	0.0	38.7	0.0	22.5	0.1	12.01
Lh	0.1	22.4	0.0	35.9	0.0	18.2	0.1	11.29
Yc	0.1	21.7	0.0	33.7	0.0	19.5	0.1	11.79
Ja	0.1	22.1	0.0	38.3	0.0	22.3	0.1	12.21
Jgs	0.1	17.6	0.1	29.5	0.0	21.4	0.1	9.29
Sc	0.1	18.8	0.0	30.1	0.0	26.4	0.1	10.89
Gx	0.1	22.5	0.0	31.1	0.0	22.8	0.0	13.35
Nc	0.1	24.7	0.0	45.9	0.0	24.4	0.0	13.55
Zs	0.1	24.5	0.0	43.4	0.0	22.1	0.1	13.59
Yof	0.1	23.4	0.0	39.4	0.0	25.4	0.1	12.90
Nd	0.1	26.3	0.0	37.4	0.0	26.2	0.0	13.96
Ln	0.1	25.0	0.1	29.4	0.0	25.5	0.0	14.30

Table 4 Changes of the gamma distribution parameters α and β in each station and season during 1959 to 2016. Z: Z values from the M-K test. When Z is bigger than 0, the trend is upward; when Z is smaller than 0, the trend is downward. When the absolute value of Z is bigger than or equal to 1.28, 1.64, and 2.32, it means that the test has passed the reliability test of 90%, 95%, and 99%, respectively. Tr: trend of α and β, increasing (↑): when the M-K statistic is positive and the confidence level is below 0.05. Decreasing (↓): when the Mann-Kendall statistic is negative and the confidence level is below 0.05. No trend (--): there is no trend detected according to the confidence level.

station	spring α Tr	spring α Z	spring β Tr	spring β Z	summer α Tr	summer α Z	summer β Tr	summer β Z	autumn α Tr	autumn α Z	autumn β Tr	autumn β Z	winter α Tr	winter α Z	winter β Tr	winter β Z
Yf	↓	-3.05	↑	2.99	--	0.74	--	0.36	--	-0.17	--	0.00	--	0.09	--	1.16
Lh	--	-1.69	↑	1.99	--	1.05	--	-0.76	--	-1.31	--	1.89	--	-0.52	--	1.01
Yc	↓	-2.76	--	1.20	--	0.74	--	1.74	--	-1.63	--	1.77	--	-0.65	--	0.74

Ja	--	-1.00	--	0.78	--	1.11	--	0.32	--	-1.92	↑	2.21	--	-0.79	↑	2.33
Jgs	↓	-2.46	--	1.37	--	-0.21	--	1.58	↓	-2.29	--	1.11	↓	-2.82	↑	3.60
Sc	↓	-2.18	--	1.62	--	0.79	--	0.89	--	-1.84	--	1.56	--	-0.43	↑	2.36
Gx	--	-1.20	--	1.19	--	-0.76	--	0.42	--	-1.49	--	0.08	--	-0.64	↑	2.35
Nc	↓	-2.42	--	1.40	--	1.91	--	0.23	--	-0.08	--	0.45	--	1.05	--	1.14
Zs	↓	-2.35	↑	2.11	--	1.67	--	0.87	--	-1.29	↑	2.75	--	0.20	--	0.71
Yof	--	-1.78	--	0.72	--	0.01	--	0.87	↓	-2.49	↑	2.69	--	-1.09	↑	2.93
Nd	↓	-2.15	↑	2.18	--	-0.39	--	1.12	--	-1.19	--	1.33	--	-1.73	↑	3.10
Ln	--	-0.83	↑	2.54	--	-0.21	--	0.08	↓	-2.13	--	0.65	--	-1.14	--	1.73

640

Table 5 Mean threshold values (mm) of 12-H in each station and seasons and their estimates obtained from the gamma distribution according data in 1959-2016. Pre_99 refers thresholds from the observed precipitation and gam_99, the estimates from gamma distribution.

station	spring		summer		autumn		winter	
	pre_99	gam_99	pre_99	gam_99	pre_99	gam_99	pre_99	gam_99
Yf	38.88	38.77	45.93	45.79	23.66	23.52	17.17	17.11
Lh	36.71	36.60	42.33	42.15	19.97	19.79	16.72	16.65
Yc	35.03	34.91	40.94	40.77	21.97	21.84	16.57	16.51
Ja	34.96	34.88	41.08	40.96	20.29	20.16	16.08	16.00
Jgs	31.58	31.48	46.97	46.86	27.32	27.15	14.31	14.23
Sc	28.85	28.79	37.59	37.49	25.78	25.58	14.31	14.22
Gx	34.32	34.23	37.17	37.05	20.02	19.87	16.87	16.77
Nc	38.39	38.24	49.09	48.89	20.04	19.84	17.38	17.31
Zs	38.06	37.97	47.98	47.78	20.87	20.71	18.39	18.29
Yof	37.92	37.81	46.23	46.03	20.90	20.68	18.04	17.96
Nd	42.33	42.22	46.05	45.84	23.72	23.52	16.92	16.84

Ln	37.89	37.76	41.76	41.56	21.20	21.06	15.99	15.88

645 **Table 6 Statistics of extreme precipitation events from 1-10 runs at Ganxian station from 2009 to 2014**

Runs	seasons	Scenario					Runs	seasons	Scenario				
		0.5	0.2	0.1	0.05	0.02			0.5	0.2	0.1	0.05	0.02
1	spring	13	9	6	6	2	6	spring	10	6	4	1	1
1	summer	12	11	9	6	5	6	summer	5	5	3	2	1
1	autumn	4	2	1	1	1	6	autumn	2	1	1	1	1
1	winter	1	1	1	1	1	6	winter	2	2	1	1	1
2	spring	11	9	6	3	1	7	spring	11	5	3	2	2
2	summer	10	8	6	4	2	7	summer	6	3	3	2	1
2	autumn	1	1	1	1	1	7	autumn	2	1	1	1	1
2	winter	1	1	1	1	1	7	winter	2	2	2	2	2
3	spring	8	7	4	2	2	8	spring	8	5	2	1	1
3	summer	9	7	4	4	2	8	summer	4	3	3	2	1
3	autumn	2	1	1	1	1	8	autumn	1	1	1	1	1
3	winter	2	1	1	1	1	8	winter	2	2	2	2	2
4	spring	9	7	4	3	3	9	spring	6	4	4	1	1
4	summer	8	5	4	2	2	9	summer	4	4	3	2	1
4	autumn	2	1	1	1	1	9	autumn	1	1	1	1	1
4	winter	2	2	2	2	2	9	winter	1	1	1	1	1
5	spring	8	7	5	2	2	10	spring	7	5	4	1	1
5	summer	5	2	1	1	1	10	summer	3	3	3	2	1
5	autumn	2	2	1	1	1	10	autumn	1	1	1	1	1
5	winter	2	1	1	1	1	10	winter	1	1	1	1	1

Table 7 Floods events recorded in Hanlinqiao hydrological station from 2009 to 2014

Year	spring	summer	autumn	winter	Total
2009	0	1	0	0	1
2010	2	1	0	0	3
2012	2	1	0	0	3
2013	1	1	0	0	2
2014	2	1	0	0	3
Total	7	5	0	0	12